

Decoding Elasticity Build-Up and Network Topology in Free-Radical Cross-Linking Polymerization: A Combined Experimental and Atomistic Approach

Shamil Saiev, David Beljonne, Roberto Lazzaroni,* and Patrice Roose



Cite This: *Macromolecules* 2023, 56, 7396–7405



Read Online

ACCESS |



Metrics & More

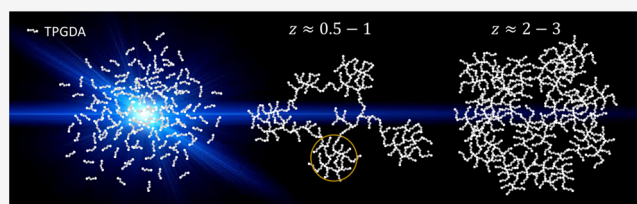


Article Recommendations



Supporting Information

ABSTRACT: The range of applications involving free-radical cross-linking processes has grown impressively over the last decades. However, in numerous fields where tightly cross-linked materials are required, the network development and its relation to the elastic properties are still a gray zone, as it is particularly challenging to design experiments that would allow validating the predictions from (often phenomenological) theoretical models or numerical simulations. Here, we report on a successful attempt to align time-resolved infrared-rheology measurements with fully atomistic simulations over the whole conversion range of an important acrylic free-radical cross-linking polymerization, unveiling the different regimes behind the elasticity build-up upon double bond conversion. Our combined experimental–theoretical approach provides an original insight into the various stages of the polymer network growth, from the earliest initiation up to final conversion. More specifically, we show that the pregel and gel formation stages are driven by the formation of branched polyfunctional polymers, which link together toward a sample-spanning network at the gel point. This regime proceeds in the postgel stage until the spatial heterogeneity in the cross-link density vanishes, leaving dangling ends as residual structural defects that then gradually connect to close the network. Following a steep transition at ultimate conversion, the elastic modulus of the network reaches the value predicted by the rubber elasticity theory in the affine limit.



INTRODUCTION

In the thrust toward a sustainable world, new material development will increasingly rely on the design and use of energy-efficient processes. With its favorable energy footprint, free-radical polymerization activated by UV light, or photopolymerization, already achieved solid acceptance in the field of industrial coatings and inks for multiple substrates including wood, paper, plastic, and glass more than two decades ago.^{1–6} The unique light-controlled resolution in space and time, along with pioneering developments in demanding areas such as dental materials or security glazing,^{7–9} raised photopolymerization to a successful, widespread technology in an expanding number of areas such as structural adhesives, bioengineering, electronics, photonics, multidimensional printing, etc.^{10–12} Today, new applications of photopolymerization linked to the energy transition, such as light-weight materials, energy storage, and encapsulation are emerging, with an enhanced focus toward renewable and recyclable precursors.^{13–17}

In contrast to step-growth polymerization mechanisms, chains and strands grow along wide-ranging structures in free-radical cross-linking owing to the random nature of radical initiation and termination processes.^{18–21} The coupling between the reaction kinetics of an active radical and its molecular host structure introduces additional spatial differentiation upon growth, characterized by fluctuations in cross-link density and connectivity imperfections such as dangling

chains and loops.^{22–24} This results in a heterogeneous network build-up, which is extremely challenging to characterize from an experimental perspective, even more so for multifunctional precursors (e.g., multiacrylate compounds) that polymerize fast owing to the gel or Trommsdorff acceleration at an early stage in the reaction.^{1,18,25}

The local structure of lightly cross-linked networks (polymer gels, (swollen) rubbers, or adhesives) after polymerization has been studied with a number of scattering and microscopic methods at submicron length scales. In particular, polymer networks formed by free-radical cross-linking showed variable degrees of structural heterogeneities depending on the amount and type of cross-linker, monomer, and solvent content, and polymerization conditions.²⁶ In these studies, evidence of domains in the final network has been related to the formation of cross-linked nanoclusters during polymerization. However, similar reports are scarce for tightly cross-linked networks, which are typically insoluble and infusible solid materials not suitable for experimental characterization. Noteworthy, a recent

Received: April 7, 2023

Revised: August 15, 2023

Published: September 5, 2023



investigation combining atomic force microscopy and X-ray scattering provided new insight into the complex structural development at the nanoscale at different steps in photopolymerization.²⁷ This was demonstrated for blends of acrylate precursors with very distinct molecular backbones, resulting in networks with an overall low to moderate cross-linking level and showing phase segregation at a submicron scale.

Independently, computational schemes were elaborated over time and could be implemented to investigate the equilibrium topology of networks generated by a free-radical mechanism and later to predict the density, the glass transition, and mechanical properties.^{28–30} In addition, topological details such as the density of the elastically effective network strands can be extracted from molecular simulations, which so far can merely be estimated approximately from experimental data within the framework of the classical statistical models.³¹ Recently, Zhong et al. proposed the real elastic network theory (RENT) that accounts for the effect of topological defects on the bulk elasticity of polymer hydrogels. By introducing the elastic effectiveness depending on the loop defect order and the topological distance of the strand from the loop, they were able to predict the shear modulus, G' , solely on the basis of molecular information.³²

In the case of free-radical polymerization, numerical experiments were conducted for well-defined molecular structures, such as hexanediol diacrylate, but so far, validation with reported experimental data was only possible at the end of the polymerization in the ultimate cross-linked state.²⁹ However, a comprehensive understanding of those systems requires the continuous monitoring of the network development during the fast transformation of a well-defined low-viscosity molecular liquid to a tightly cross-linked network, which is still an unmet experimental challenge. Yet, significant technical progress was achieved recently in recording the viscoelastic evolution of a fast cross-linking network, additionally coupled to time-resolved spectroscopic data in some cases.^{33–38} The sensitivity of the elastic modulus provides an indirect but effective probe of the overall network structure, and the relationship between the elastic modulus and the network topology has been investigated since the early days of polymer physics.¹⁸

Here, we address this issue through a joint experimental/modeling approach combining simultaneous time-resolved infrared-rheology measurements with atomistic molecular dynamics simulations, which offer a new perspective on the formation of tightly cross-linked networks (here applied to a well-defined diacrylate precursor) for a rapid photoinduced free-radical polymerization process. We stress that the simulations have been designed and conducted to reproduce as closely as possible the experimental conditions (i.e., soft initiation conditions, quasi-equilibrium), hence providing a detailed and robust mechanistic description of the evolution of the network topology with conversion. We show experimentally that, at temperatures sufficiently high to avoid vitrification over the course of the polymerization, the elasticity build-up after gelation unveils three distinct regimes as a function of double bond conversion. These regimes match remarkably well the three well-defined stages of the topology development observed from molecular modeling simulations. The formation and connection of highly functional polymer structures play a key role in the network and concomitant elasticity development up to half conversion. Subsequently, a transition to a uniform percolation regime occurs. Close to full conversion, the elastic modulus ramps steeply toward the affine limit prediction of the

rubber elasticity theory, correlating with a decline of the thermal fluctuation amplitude of the cross-link points.

METHODS

Materials. Tripropyleneglycol diacrylate (TPGDA, $M_w = 300 \text{ g mol}^{-1}$) was supplied by Allnex (Belgium). High purity was achieved by complete acrylation of the residual hydroxyl groups using a slight molar excess of acryloylchloride and triethylamine for neutralization. The reaction was conducted in dichloromethane at 60 °C for 24 h. Next, the organic phase was washed three times with water in order to remove any salt trace. The purity was confirmed by standard GC-FID chromatography and FTIR spectroscopy.

For the photopolymerization experiments, a photoinitiator (1-hydroxycyclohexyl phenyl ketone, HCPK, Irgacure 184, BASF, $M_w = 204.3 \text{ g mol}^{-1}$) was added to the TPGDA precursor at $\approx 0.1 \text{ mol } \%$ (i.e., $[\text{HCPK}] \approx 7.0 \text{ mmol L}^{-1}$) with respect to the double bond content. The molar extinction coefficient ϵ of HCPK was determined by UV-vis spectroscopy from a 0.1 w/w% solution in acetonitrile. At a wavelength of 365 nm, the value $\epsilon_{365} = 37.5 \text{ L mol}^{-1} \text{ cm}^{-1}$ was determined.

Experimental Monitoring of the Cross-Linking Process.

Photorheology coupled with time-resolved FTIR-MIR spectroscopy was used to follow the polymerization of the TPGDA precursor upon photoactivation. The small-strain viscoelastic properties were monitored in oscillatory deformation along with the spectral changes in the MIR range. For this purpose, an MCR302 rheometer (Anton Paar) was equipped with a UV-transparent quartz cylinder (diameter 8.3 mm) mounted in a steel shaft as the upper body of a parallel plate configuration (Supporting Information 1). The bottom side of the quartz cylinder in contact with the sample was sanded to improve adhesion by increasing the surface roughness. Light emitted from a UV-LED at a wavelength of 365 nm (Thorlabs) was guided optically onto a mirror at the top of the shaft and redirected through the quartz cylinder toward the sample, filling a gap of 300 μm between the plates. The bottom plate of the rheometer was fixed in a Peltier heating element for temperature control. An attenuated total reflectance mid-infrared (ATR-MIR) monitoring probe was fitted within a circular opening machined in the center of the plate. The IR probe was connected to an MCT detector of a Tensor 27 FTIR spectrometer (Bruker). IR spectra were acquired at the highest rate ($\approx 2.3 \text{ s}^{-1}$) in the wavenumber range with the highest signal-to-noise ratio, i.e., between 650 and 1800 cm^{-1} at a resolution of 2 cm^{-1} . The consumption of the acrylate double bonds was estimated from the area of the absorption peak at 810 cm^{-1} (τ (= CH_2), area A_{810}) scaled with respect to the area of the absorption band of the carbonyl stretching at 1720 cm^{-1} (ν ($\text{C}=\text{O}$), area A_{1720}) in order to compensate for measurement variations. The fractional double bond conversion was estimated as $p(t) = 1 - (A_{810}/A_{1720})_t / (A_{810}/A_{1720})_0$.

The photopolymerization step was conducted at 90 °C in order to achieve high conversion rates in nonvitrified conditions. Prior to the measurement, dissolved molecular oxygen was removed by bubbling nitrogen gas through the sample for 20 min. The viscoelastic properties were measured every 0.5 s using an oscillatory strain with an amplitude of 0.2% and a frequency of 10 Hz. The sample was exposed for 10 min to UV light at an intensity of 10 mW cm^{-2} at a sample location (measured using a high-resolution thermal power sensor of Thorlabs). While insignificant for the phase angle, the aperture in the bottom plate increased the apparent shear modulus by a factor ≈ 2 relative to the absolute values obtained with a flat plate without the IR probe. The moduli values were corrected accordingly.

For a reliable correlation of the viscoelastic and the spectral data in a TR-MIR photorheology experiment, it is a prerequisite to achieve uniformity of the absorbed light intensity and, hence, the initiation rate across the sample volume during polymerization. Whereas the lateral homogeneity of the incident beam is easily verified experimentally, the light absorption along the incident path is estimated from the molar concentration and the molar extinction coefficient of the photoinitiator at 365 nm. As the ATR crystal has a triangular shape with its top at the level of the bottom plate (cf. Supporting Information 1), the light absorbed by the photoinitiator should be uniform down to the bottom end of the crystal surface ($\approx 2 \text{ mm}$ below the shear gap). According to

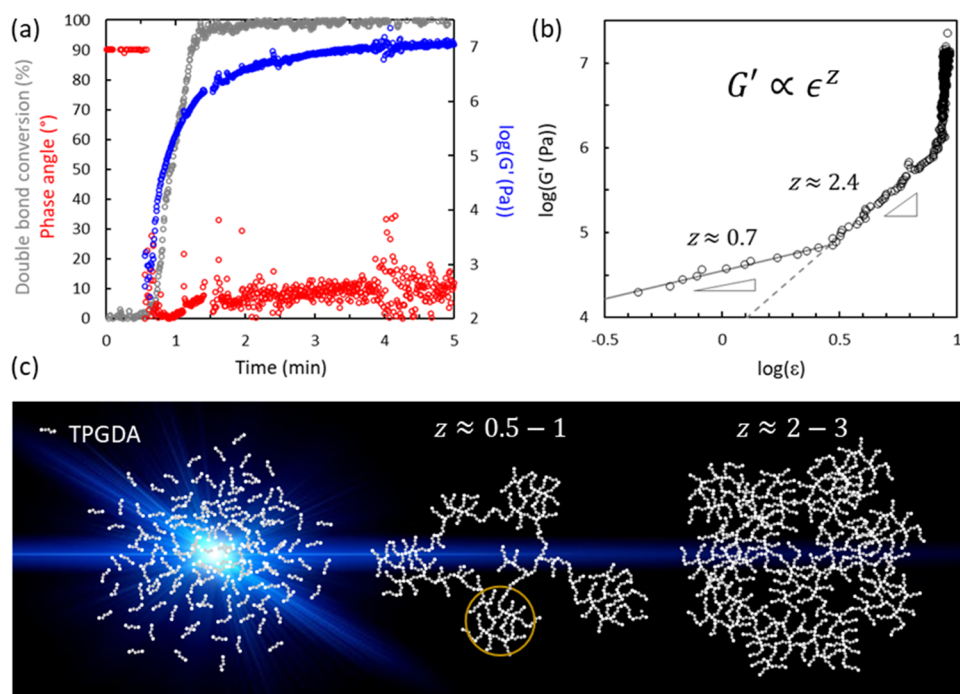


Figure 1. (a) Plot of the elastic shear modulus G' , the double bond conversion, and the viscoelastic phase angle as a function of time upon UV exposure for TPGDA at 90 °C. (b) Double logarithmic plot (base 10) of the shear modulus G' vs the reduced bond probability $\epsilon = |p - p_c|/p_c$ using the value $p_c \approx 0.1$ as predicted from the simulations. The exponents of the respective power law regimes are reported. Extrapolation of the second regime toward zero modulus (dashed line) returns the conversion value at the gel point. (c) Schematic representation of the initial monomer bath exposed to light (left), the stage of connected branched polymers after the gel point (center), and the percolating cross-linked network (right).

the law of Beer–Lambert, the absorbed light intensity reads as $I_a = I_0(1 - e^{-\alpha_{365}})$, with $\alpha_{365} = 2.303\epsilon_{365}[\text{HCPK}]d$ and I_0 is the incident photon flux, which is well approximated as $I_a \approx I_0\alpha_{365}$ for $\alpha_{365} \ll 1$, expressing a constant number of absorbed photons per incremental depth interval. While this “thin-film approximation” is clearly valid at the top of the ATR crystal where $\alpha_{365} \approx 0.018$, it deviates by 7% at the bottom end where $\alpha_{365} \approx 0.14$. Thus, it is reasonable to assume that the average conversion probed by the ATR crystal reflects the conversion of the precursor at the level of the shear gap. The initiation rate of the photopolymerization process can be estimated here from the decomposition rate of the photoinitiator, i.e., $R_d = \varphi_d I_a/d$, where φ_d is the quantum yield and d is the depth of the volume element. At the level of the gap, an upper bound for the initiation rate is then $R_{d,\max} = 2.303\epsilon_{365}[\text{HCPK}]I_0$, assuming $\varphi_d = 1$. According to the experimental conditions, i.e., incident light at 365 nm with an intensity of 10 mW cm^{-2} , $R_{d,\max} = 1.8 \cdot 10^{-5} \text{ mol L}^{-1} \text{ s}^{-1}$.

Molecular Dynamics Simulations. The construction and molecular dynamics simulations of the TPGDA networks were performed using the Materials Studio 7.0 (Biovia) commercial simulation package. The Dreiding force field was adapted to represent at best the intra- and interatomic interactions of the studied molecules³⁹ (Supporting Information 2). The nonbonded terms include hydrogen bonding, electrostatic, and van der Waals forces. The latter were calculated by means of the Lennard-Jones (12-6) potential function, whereas the Coulombic contribution is evaluated using the group-based summation because of its capacity to reduce energy fluctuations and computational time. The cutoff is set at 1.2 nm for both interactions. The atom charges were computed using the Gasteiger iterative partial equalization method.⁴⁰ During the simulations, the Parrinello–Rahman barostat (at atmospheric pressure) and the Nosé–Hoover–Langevin (NHL) thermostat (with a Q ratio of 0.01) were employed to control the pressure and the temperature of the simulation box, respectively.⁴¹

RESULTS

Conversion Scaling of the Elastic Build-Up in Free-Radical Cross-Linking Polymerization.

Tripropyleneglycol diacrylate (TPGDA) is widely used in UV-curable formulations as a versatile reactive solvent (“diluent”) owing to its low viscosity (10 mPa s). With two acrylate double bonds, this small molecule acts as an efficient four-functional cross-linker in a radical polymerization process. Upon complete reaction of the double bonds, the glass-transition temperature (T_g) of the cross-linked TPGDA is ≈ 70 °C according to the loss modulus maximum (Supporting Information 3). The transformation from the low-viscosity liquid into a tightly cross-linked network following a fast photoinduced free-radical polymerization has been monitored from a chemical and a viscoelastic perspective in a synchronous time-resolved approach (using time-resolved infrared photorheology). By setting the temperature at 90 °C (i.e., above T_g), vitrification was avoided along the course of the polymerization. A uniformly distributed radical population was achieved in steady state at a low initiation rate of the order of $10^{-5} \text{ mol L}^{-1} \text{ s}^{-1}$. As center-of-mass diffusion slows down quickly within a few percent of conversion for small multiacrylate precursors, radical termination is primarily controlled by reaction–diffusion over most of the polymerization process.^{25,42} The ratio of the kinetic coefficients between termination and propagation is around $k_t/k_p \approx 30\text{--}40$ for acrylates in this regime, where the value of k_p is typically of the order of $10^4 \text{ M}^{-1} \text{ s}^{-1}$ for diacrylates.^{25,42} From these values, one can readily estimate the ratio between the double bond and radical concentrations to be $\approx 1.0 \times 10^6$ and down the line also the average kinetic chain number $\nu \approx 10^4$, which expresses the mean number of double bonds that have reacted per radical before termination takes place. This order of magnitude suggests that the structural development of the network can be modeled

by assuming the presence of a single radical in a pool of double bonds (*vide infra*).

The rapid transformation in time of TPGDA upon UV exposure is illustrated in Figure 1, where the shear modulus and the double bond conversion are plotted vs time at 90 °C (in oxygen-free conditions). The sudden drop of the phase angle at the onset of double bond conversion indicates that the viscoelastic gel point is reached at a low conversion.⁴³ In contrast to the fast conversion ramp (gray dots), the shear modulus (blue dots) follows a rather gradual growth up to a limiting value of $\approx 10\text{--}15$ MPa at full conversion. Gelation theories typically predict scaling relationships of the form $G_\infty \propto \epsilon^z$ for the equilibrium elastic modulus in terms of the reduced bond probability $\epsilon = |p - p_c|/p_c$, where p_c stands for the bond probability or fractional conversion at the gel point (also referred to as critical conversion). Scaling exponents usually reflect structural and dynamical self-similarity, with $z \approx 2.6$ and 3 for predictions based on critical and mean-field percolation theories, respectively.^{18–20}

As confirmed below, *a priori* topological knowledge from the simulation data indicates that small highly functional macromolecules (further referred to as branched polymers) are formed initially before connecting together, mainly by propagation, and turning in a weak incipient gel at $p_c \approx 0.1$, in particular, for radicals in a large pool of double bonds. Using the latter prediction as the best guess for the experiment, the correlation between the concurrent data sets of G' and ϵ in Figure 1 reveals three clear regimes characterized by two power law behaviors after gel formation and the final steep increase within the last stage of bond conversion. The scaling factor for the build-up of the network elasticity at the low conversion side is $z \approx 0.7$, which reflects the continuance of the structural growth mode driven by the linking of the polyfunctional branched polymers mutually or to the network backbone. At this stage, isolated polymers are continuously formed in the polymerization bath upon constant UV exposure. It is further stressed that, similar to a solvent, unreacted (or “free”) TPGDA molecules result in a weak softening effect of the elastic properties of the polymer network.²⁰ Upon consumption of free monomer at low conversions, a scaling exponent $z_{\text{mon}} \approx 0.3$ is predicted for G' in the assumption of a statistical polymerization in θ conditions.

This first modulus regime is maintained up to a fractional conversion of $p \approx 0.4$ where a second regime kicks in with a much higher slope $z \approx 2.4$, reminiscent of a bond percolation process tightening the network efficiently. Noteworthy, the extrapolation of the second regime toward zero modulus returns the conversion value at the gel point. Finally, the modulus grows by more than 1 order of magnitude in the ultimate transformation close to complete conversion. The final experimental value is close to the shear modulus value estimated in the affine limit of the rubber elasticity theory, i.e., $G_\infty \approx 10$ MPa, using an initial double bond content of 6.7 mol kg⁻¹ for the studied TPGDA precursor. Consistent with a thermosetting behavior, the experimental shear modulus shows a constant value at temperatures beyond the glass transition (Supporting Information 3).

Topological Analysis of Free-Radical Cross-Linking Polymerization. Molecular dynamics (MD) simulations provide a solid framework to investigate the gelation mechanism and the formation of acrylate-based polymer networks from a topological perspective. For the construction of polymer networks, different multistep methods were developed in the past.^{44–46} Among these, the progressive polymerization

approach based on distance criteria was extensively applied to cross-linked networks formed by step-growth polymerization.^{47–52} Fewer studies have been reported for the free-radical chain polymerization of multifunctional unsaturated precursors.^{29,44,53} The modeling of the polymerization process and the tools for network analysis were applied in this work built on previous structure–property studies in the field of thermosets.^{54–56} We adapted the simulation algorithm in order to reproduce appropriately the propagation of the radical after each reaction step. In the model, the structural development along the living polymerization process was followed for one radical in a pool of TPGDA molecules, as suggested by the experimental results described above (termination steps and chain transfer are neglected in the model). However, for extrapolation purposes and consistency analysis, the model structures were prepared for a range of initial TPGDA molecules ($N_{\text{TPGDA}} = 800, 400, 200, 100, 50,$ and 25) in the presence of a single radical center. The results of the topological development are reported against the ratio $r = n/N$ of the radical to double bond numbers, n and N , respectively (i.e., for one radical $r = 1/2N_{\text{TPGDA}} = 0.0625, 0.125, 0.25, 0.5, 1,$ and 2 mol %, respectively). The validity of the “one-radical” approach was verified by comparison to simulations at similar ratios r but conducted with two initial radicals (i.e., $r = 2/2N_{\text{TPGDA}}$). The simulated radical polymerization focuses on the growth of the single main chain involving the gradual reaction of the diacrylate monomers up to full double bond conversion. Irrespective of the initiation details, the approach closely mimics the polymer development in the experiment when one radical, after creation, propagates across a very large number of double bonds before termination. In addition, avoiding vitrification effects warrants a direct comparison between experimental and simulation results. This modeling strategy is in stark contrast with former simulation studies typically conducted with fairly high radical concentrations (primarily aimed at reducing the required computational cost, which was not restricted here).^{28,29} At high radical concentrations, however, experiments monitoring the fast radical polymerization cannot be conducted owing to limitations in instrumental response time, hence preventing an unambiguous connection between the theory and experiment. Following the low radical approach described here, modeling of the polymer structures provides a topological map of the network build-up for comparison with the experimental modulus data from the pregel stage to the gel point across the complete postgel phase.

Pregel and Incipient Gel Formation. Gelation is defined by the appearance of the three-dimensional infinite insoluble network during polymerization. Scanlan and Case have defined the active part of the gel as being composed of “cross-linking junctions or cross-links” joined by at least three paths to the infinite network and “elastically effective network strands” terminated by cross-links at both ends.^{57,58} Because of the localized nature of the free-radical cross-linking, the early stages of the polymerization lead to intramolecular chain cyclization events and the formation of highly functional polymers.²⁶ Further polymerization results in the intermolecular bridging of those branched polymers, which start to form a sample-spanning infinite network at the gel point. During the analysis of the growing chain(s), the emergence of an infinite structure can be detected from its undefined gyration radius as it can only be computed for a finite polymer structure. The simulation algorithm developed earlier for step-growth polymerization⁵⁵ was adapted for radical polymerization here and is described in Supporting Information 4.

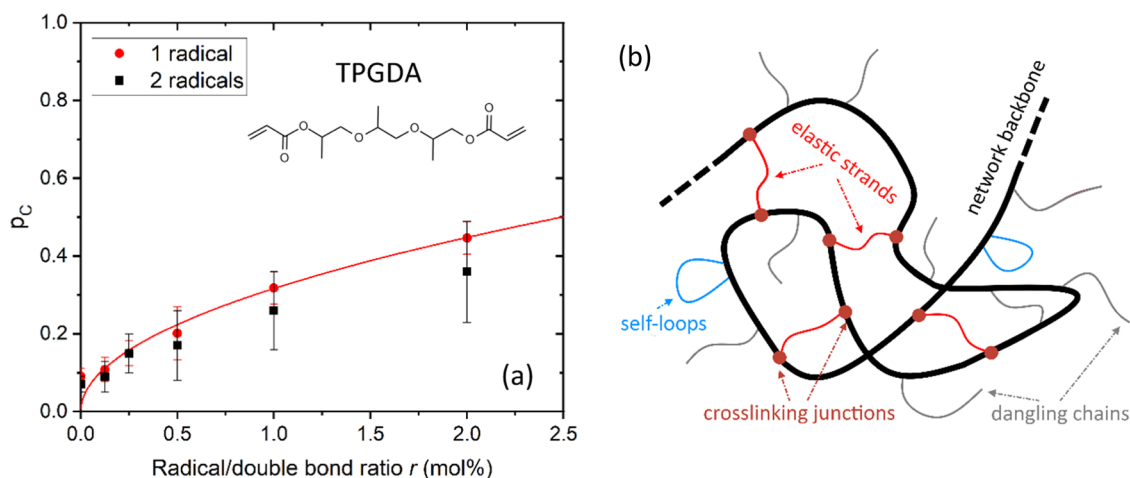


Figure 2. (a) Critical conversion p_c as a function of the radical/double bond ratio r for the formation of the gel using either one (orange circle solid) or two starting radicals (solid squares) in the simulation box. The line highlights the square-root behavior predicted from models based on statistical mean-field approximations. (b) Schematic representation of the network backbone and three types of structural chains (elastically effective network strands, dangling chains, and self-loops) along with the cross-linking junctions.

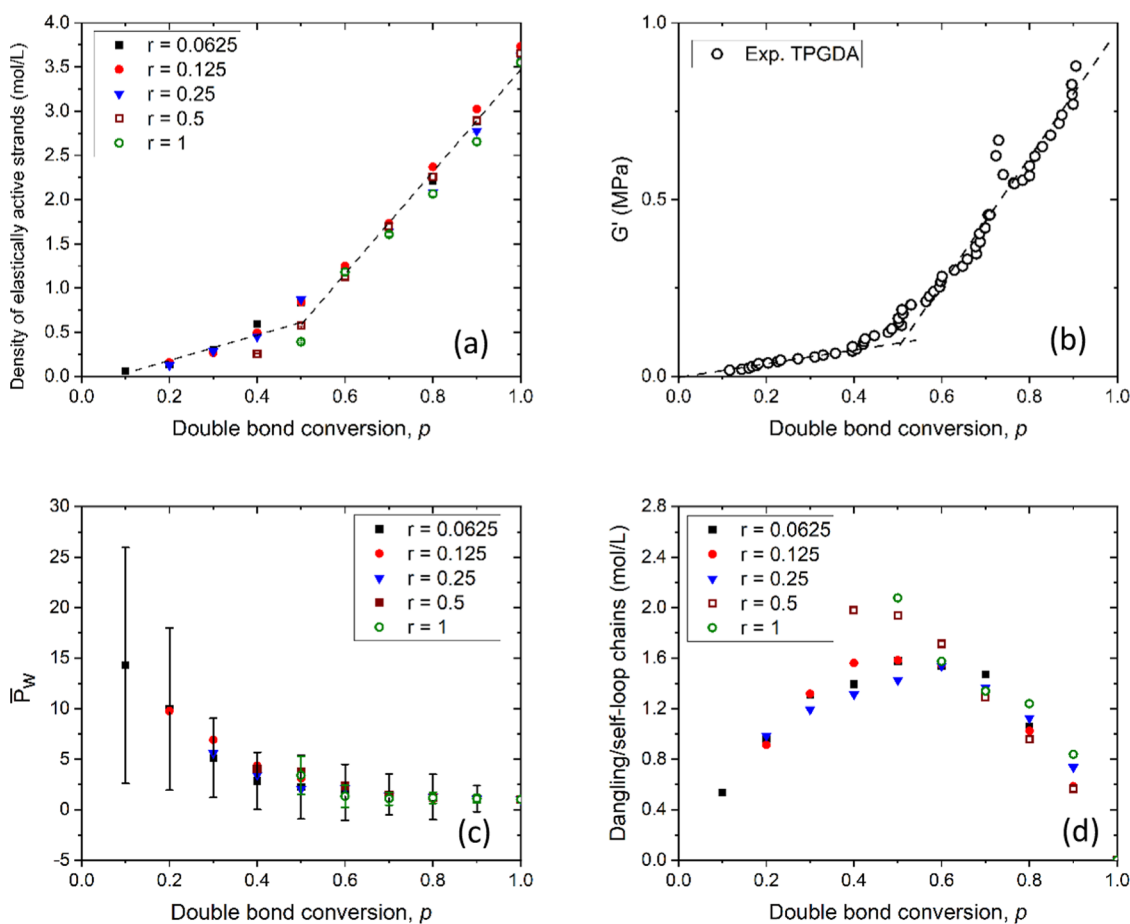


Figure 3. Structural characteristics of the cross-linked main chain. (a) Density of elastically active network strands vs double bond conversion p . (b) Experimental shear modulus up to a double bond conversion $p \approx 0.9$ represented on a linear scale. (c) Weight-average degree of polymerization \bar{P}_w of the elastically active network strand. The standard deviation of \bar{P}_w is provided as error bars for the simulations at $r = 0.0625$ and 1 mol %. (d) Concentration of structural defects (total of dangling and self-loop chains). The results are shown for numerical simulations conducted at different radical/double bond ratios r (in mol %).

Figure 2a shows the dependence of the critical conversion p_c for increasing radical/bond ratio r . The overall behavior of p_c follows a square-root dependence in agreement with mean-field predictions for free-radical cross-linking systems. In particular,

Korolev et al. derived criteria for the critical conversion from the moments of a generating function including the number of monomers, functionality, and active centers of the growing polymers.⁵⁹ Typically, for fast initiation, $p_c = \sqrt{r/(\bar{f} - 1)}$,

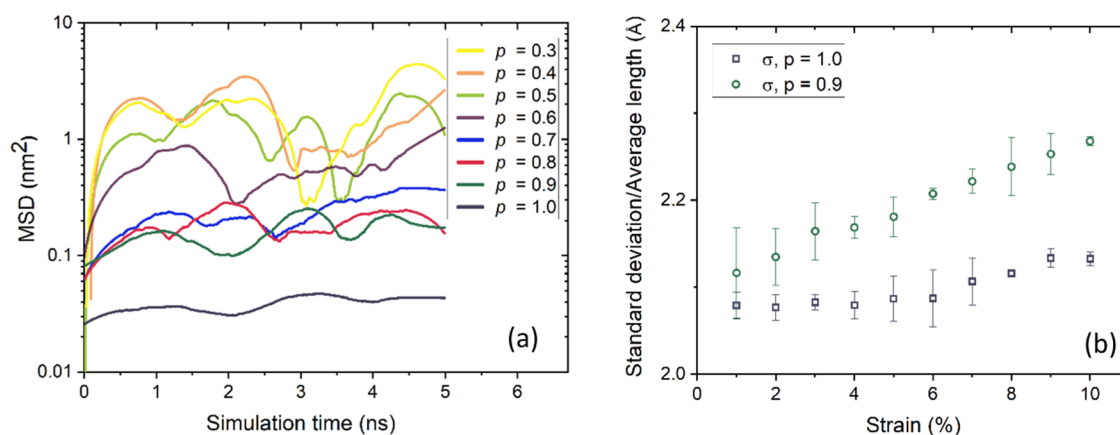


Figure 4. Fluctuations of the cross-links and transition to the affine network. (a) Mean square displacement (MSD) of atoms in the structural cross-links after gelation. The curves are displayed as average results for all of the structural cross-links smoothed over 100 points using the Savitzky–Golay method. (b) The standard deviation of the average length of the elastic chains as a function of the strain, averaged over three different structures at $p = 0.9$ and 1.0 .

where \bar{f} is the average number of double bonds in the monomer ensemble. In the limit where $r \rightarrow 0$, the agreement no longer holds and a limiting value $p_c \approx 0.1$ is achieved when radicals are highly diluted within a large number of monomers. Consistent with the experimental conditions as mentioned before, the latter value was used in Figure 1b to estimate the reduced bond probability. Figure 2a also highlights similar trends for p_c when predicted following a one-radical or a two-radical scenario, which supports the assumption of independent molecular growth. Not surprisingly, the agreement is close at the lowest radical/double bond ratios but we note some deviation between the two approaches at higher ratios, chiefly attributed to difficulties in obtaining uniform distributions of the two starting radicals in the (small) simulation boxes. At the lower end of the stoichiometric window, more specifically at $r = 0.0625$, 0.125 , and 0.25 mol % (larger boxes), the simulations show that intramolecular reactions occur during the formation of the branched polyfunctional polymer chains before the actual gel formation. Typically, intramolecular reactions start after the polymerization of approximately 30 TPGDA molecules and lead to cycles and cross-links within the polymer. At low r , radicals primarily grow by propagation in a nearly infinite pool of monomers, suggesting that the polymer growth will exhibit the same features for larger-scale models. A high r , the polymerization process precipitates the formation of an infinite network, driven by the intermolecular interactions among the extending polymer chains. As a result, the development of the infinite network ultimately predominates without the formation of pre-cross-linked branched polymers.

Postgel Network Development. After the gel point, the elasticity of the network develops according to the formation of elastically effective network strands. Tracking the type and number of chains helps in understanding the structural imperfections and local fluctuations in the network, which affect the elastic behavior of the overall network. As before, elastically active cross-links are defined as junction points with at least three paths leading to the infinite structure and allow us to classify the chains in four categories based on their structural features: (i) elastically active strands, which are segments attached to active cross-links at both ends, (ii) dangling chains attached to the main polymer network by only one end and, hence, not fully incorporated into the network structure as the active chain, (iii) self-loops, with both ends connected to the

same junction point forming a cyclic structure, and (iv) free chains not connected to the rest of the network and part of the sol fraction. The algorithm to identify the chains involves several steps: (i) assigning the same name to new linked pairs of atoms during curing, (ii) establishing the linkage map using the names of the reacted atoms between all of the molecules in the largest fragment, (iii) identifying linear chains and corresponding chain lengths, and (iv) finally, classifying each monomer unit into one of the four categories: free chain, dangling end, elastically active chain, or self-loop, as well as enumerating the active cross-links (cf. Figure 2b). The structural heterogeneity that follows from the spatial distribution of the cross-links leads to a broad distribution of elastic strand lengths.²⁶ From a detailed analysis of the simulated structures using a custom-made algorithm, the number of active cross-links, the density of elastically active network strands ν_e , the number of structural defects, and the dispersity of the elastic chains were determined at various steps of double bond conversion (Figure 3).

Figure 3a reveals that the density of elastically active network strands follows a piecewise linear growth as a function of the double bond conversion marked by a slope change at $p \approx 0.4$ – 0.5 regardless of the size of the simulation box. The slope transition correlates remarkably well with the observed regime change for the experimental shear modulus (Figure 3b, which is a linear representation of Figure 1b as a function of conversion), suggesting a qualitative but not straightforward quantitative relationship between these quantities, as discussed later. The weight-average degree of polymerization \bar{P}_w of the elastically active network strands, along with the standard deviation, is plotted in Figure 3c for various simulated structures. Upon double bond conversion, \bar{P}_w is characterized by a marked decrease between the gel point and $p \approx 0.4$ – 0.5 , eventually converging toward the value of a single monomer unit beyond $p \approx 0.7$ (which means the TPGDA monomers act as single elastic strands in the network, not in sequences of monomers anymore). The standard deviation of \bar{P}_w further probes the network uniformity and is here illustrated for the low and high radical/double bond ratios, $r = 0.0625$ and 1 mol %, respectively. At the lowest ratio $r = 0.0625$ mol % (largest error bars), the random development of branched, intramolecularly cross-linked, polymers before gelation (as discussed earlier) further echoes in a pronounced network heterogeneity, which lasts up to $p \approx 0.9$. The persisting network heterogeneity provides a

rationale behind the motional freedom of the cross-links up to very high conversion levels as discussed later. In contrast, the network develops uniformly from the start at the highest ratio r (error bars within symbol at low conversion). Finally, Figure 3d highlights the aspect of network defects represented by the concentration of dangling chains and self-loops. Irrespective of the radical/double bond ratio, the number of structural defects grows after gel formation up to a conversion of $p \approx 0.5$ – 0.6 and decreases gradually beyond $p \approx 0.7$. The defects are predominantly dangling chains with self-loops only contributing to a small extent (2–3%). It is further emphasized that even at a conversion $p = 0.9$, there is still a non-negligible number of defects present in the network, which only disappear completely at full conversion ($p = 1$). The presence of these defects not only contributes to an overall reduction of the cross-link density but also introduces additional degrees of freedom to the fluctuation of the cross-links (i.e., a free volume increase).

A uniform closure of the network leads to motional and free volume constraints. As shown in Figure 4a, monitoring the mean square displacement (MSD) of the elastically effective strands supports the picture that structural defects and cross-link heterogeneity impart motional freedom at conversions below $p = 0.6$. A strong reduction of the MSD (by 1 order of magnitude) is noticed between $p = 0.6$ and 0.7 . Upon further conversion to $p = 0.9$, the observed depletion of structural defects (cf. Figure 3d) does not alter the fluctuation level further. At complete conversion, however, a second major drop takes place, leading nearly to the motional arrest of atoms in the network. These findings corroborate the analysis of Torres-Knoop et al. where a similar transition was identified at high conversion for diacrylate networks using graph theory for the structural analysis. A marked enhancing effect was demonstrated for the glass-transition temperature beyond this point.³⁰

The simulated structures at $p = 0.9$ and 1.0 were additionally subjected to a uniaxial tensile deformation in order to probe the effect of the fluctuation level of the network junctions on the elastic response of the strands. The average strand length increases linearly with the strain for both conversion degrees. However, whereas the standard deviation increases with strain at $p = 0.9$, it remains remarkably constant for the fully polymerized network in the elastic regime, implying a uniform deformation of the elastic strands, which is consistent with the classical affine model assumption (Figure 4b). The loss in motional freedom beyond $p = 0.9$, along with the improvement in network uniformity, provides a rationale behind the increase of the shear modulus G' by nearly 1 order of magnitude in the final stage of the polymerization (see Figure 1b).

DISCUSSION

Network Topology and Elasticity. As illustrated for the model diacrylate TPGDA here, free-radical polymerization inherently leads to a polydisperse ensemble of molecular entities at an early stage that connect into a sample-spanning network at a low conversion, concurrently initiating the build-up of the macroscopic elastic modulus. The modulus is particularly sensitive to the early development of branched polymers that, once connected as an elastic network, act as nodes in a less cross-linked matrix. Mark and co-workers documented experimentally the effect of elastic strand dispersity on the mechanical properties of defect-free networks by mixing short and long segments between cross-links.^{60,61} In comparison to uniform networks, a heterogeneous one with interconnected clusters loses capacity to store elastic stress and develops nonlinear

characteristics typical for filled materials in terms of loading (e.g., filled elastomers).^{62,63} As an illustrative example, Felderhof and Iske predicted theoretically a shear modulus of the form $G_\infty = G_m(1 + 1.5\chi)/(1 - \chi)$ for rigid spheres with a volume fraction χ in an elastomer matrix with modulus G_m .⁶⁴ Strictly valid for hydrodynamic reinforcement, this expression reflects the weak filling effect of hard spheres over a broad range of volume fractions.^{65,66} Next to the spatial distribution and efficiency of strands at conversions below 0.5 (Figure 1b), the network is additionally diluted by free monomer and dangling ends (akin to a swollen heterogeneous polymer gel), which overall results in a modulus build-up characterized by a power law with an exponent smaller than one.

While the polymerization of TPGDA predominantly generates nonelastic dangling ends in the first regime, the situation changes drastically in the second one (scaling exponent $z \approx 2.4$) where dangling ends are effectively incorporated into the network as elastic strands, alongside reducing the cross-link heterogeneity. The elasticity of uniform defect-free polymer networks has been described by the classical statistical theory of rubber elasticity and predicts a linear relationship between the equilibrium moduli G_∞ and ν_e and the number density of the elastically active strands, according to $G_\infty = \phi\nu_e RT$, where R is the gas constant and T is the absolute temperature. The front factor ϕ is weakly dependent on the assumed constraint level of the junction points, ranging from 1 for an affine network to $1/3$ for a phantom network with a cross-link functionality $f = 3$.^{20,21} The affine model assumes that cross-links are firmly attached to their positions and strands deform proportionally to the macroscopic deformation of the network. In the phantom case, the condition of affinity is relaxed to the mean position of the junctions, allowing junction fluctuations to capture any excluded volume effects of the chains. The latter approach ignores any description of chain statistics and volume exclusion as such, and more elaborated models have been proposed later on.^{18,20} Experimental data have usually shown better agreement with predictions from the phantom model compared to the affine one. The reduction of the elastic strands is a direct manifestation of structural defects. Additionally, this study demonstrates that these defects induce a transition from phantom to affine models, an effect driven by network fluctuations. Furthermore, the combination of network heterogeneity and the structural defects has a profound impact on the shear modulus magnitude, ultimately leading to deviation from the theoretical predictions. Furthermore, the molecular modeling indicates that the elastic effectiveness of the strands depends on the fluctuations of the network junctions. For the fully polymerized network, the cross-links are pinned in a uniform structure conforming to the ideal affine assumption. Consistently, it appears that the experimental value of the ultimate shear modulus is remarkably well predicted from the statistical theory using the density of elastic strands found by simulations ($\nu_e = 3.50$ – 3.75 mol L^{-1}), i.e., $G_{\text{sim}} \approx 11 \text{ MPa}$ at 90°C . However, at $p = 0.9$, the experimental shear modulus is much lower, i.e., $G_{\text{exp}} \approx 1 \text{ MPa}$ compared to $G_{\text{sim}} \approx 8.5 \text{ MPa}$ calculated using the affine model (for $\nu_e = 2.65$ – 2.95 mol L^{-1}) and is closer to $G_{\text{sim}} \approx 2.8 \text{ MPa}$ predicted in the phantom limit. The different behavior close to full conversion can be reconciled by considering that the presence of topological defects decreases the elastic effectiveness of the strands, inducing additional fluctuations in the cross-link background, as suggested in Figure 4a. The reduction of this (thermal) fluctuation level in the range $p = 0.9$ to ≈ 1.0 translates into an increase of the elastic modulus

according to a transition from phantom conditions toward the affine limit. Akagi et al. observed a similar transition by varying the initial polymer volume fractions φ_0 and M_n of the tetra-PEG gels.⁶⁷ Below $p = 0.9$, any source of the leftover network heterogeneity or structural imperfections prompts motional freedom on a molecular scale that ineluctably affects the shear elastic modulus, resulting in significant discrepancies between the experimental results and the classical elastic models.^{32,68,69}

For applications involving thermosets, the average cross-linking density is often considered as the single important parameter to control the glass-transition properties, solvent resistance, and transport properties of the material in service. The cross-linking level and network imperfections also strongly affect the strength and failure properties of the cross-linked material in the final state. In addition to those features, elasticity and dissipation properties can play an important role during processing, possibly at an intermediate stage (such as in thermoforming applications), and are intimately related to the details of the network at a certain point along its formation.

CONCLUSIONS

We have clearly shown that the construction of a network by free-radical cross-linking develops along different regimes where the relation between the shear modulus in the elastic plateau at high temperatures and the cross-linking density is far from straightforward. This has been established from the topological understanding behind experimental viscoelastic data for a well-defined diacrylate (TPGDA), where bond conversion operates as the unifying parameter between the experiment and modeling.

A unique rheological experiment allowed us to monitor the shear modulus growth upon conversion in photoinduced polymerization conditions. After gelation, three distinct regimes were evidenced, with the first two scaling as power laws of the conversion with exponents $z \approx 0.7$ and 2.4 , respectively. Our molecular modeling investigations show that the relative number of active centers per double bond defines whether the incipient macroscopic gel proceeds via the connection of branched, intramolecularly cross-linked, polymers formed in the pregel stage or not. After the gel point, elastic cross-linking first develops slowly as single-bonded molecules (dangling ends) and loops accumulate in the network upon polymerization. This trend culminates at a conversion of around 0.5 , next followed by the percolating closure of the network where dangling ends form elastically active strands by linking to the network, in line with the regime change to a much higher exponent observed for the shear modulus. While negligible in terms of cross-linking density, the presence of residual structural defects close to complete conversion still has a paramount effect on the fluctuation level of the cross-links in the lattice, which virtually vanishes only at full conversion. This key finding provides a rationale for the strong modulus increase at the very end of the polymerization, in line with a change from phantom to affine conditions, as predicted theoretically.

ASSOCIATED CONTENT

Supporting Information

The Supporting Information is available free of charge at <https://pubs.acs.org/doi/10.1021/acs.macromol.3c00644>.

- (1) Representation of MIR photorheology coupling; (2) parameters of the Dreiding force field; (3) viscoelastic properties of polymerized TPGDA as a function temper-

ature; and (4) description of the polymerization algorithm (PDF)

AUTHOR INFORMATION

Corresponding Author

Roberto Lazzaroni – Laboratory for Chemistry of Novel Materials, Materials Research Institute, University of Mons – UMONS, Mons 7000, Belgium; orcid.org/0000-0002-6334-4068; Email: roberto.lazzaroni@umons.ac.be

Authors

Shamil Saiev – Laboratory for Chemistry of Novel Materials, Materials Research Institute, University of Mons – UMONS, Mons 7000, Belgium; orcid.org/0000-0001-8914-5828

David Beljonne – Laboratory for Chemistry of Novel Materials, Materials Research Institute, University of Mons – UMONS, Mons 7000, Belgium; orcid.org/0000-0002-2989-3557

Patrice Roose – Allnex Belgium SA/NV, Drogenbos 1620, Belgium; orcid.org/0000-0003-2768-701X

Complete contact information is available at: <https://pubs.acs.org/10.1021/acs.macromol.3c00644>

Author Contributions

The manuscript was written through contributions of all authors. All authors have given approval to the final version of the manuscript.

Notes

The authors declare no competing financial interest.

ACKNOWLEDGMENTS

This work was supported by FNRS within the PROSPECT project of the FLAG-ERA-JTC2019 program (Grant Number 34817084). The molecular modeling activities in Mons are supported by FNRS (Consortium des Équipements de Calcul Intensif—CÉCI, under Grant 2.5020.11) and by the Walloon Region (ZENOBÉ Tier-1 supercomputer, under Grant 1117545). D.B. is an FNRS Research Director.

REFERENCES

- (1) Pappas, S. *UV Curing: Science and Technology*; Plenum Press: New York, 1992.
- (2) Kloosterboer, J. G. Network Formation by Chain Crosslinking Photopolymerization and its Applications in Electronics. In *Electronic Applications. Advances in Polymer Science*; Springer: Berlin, 1988; Vol. 84.
- (3) Schwalm, R. *UV Coatings: Basics, Recent Developments and New Applications*; Elsevier: Amsterdam, The Netherlands, 2006.
- (4) Fouassier, J. *Photoinitiation, Photopolymerization, and Photocuring: Fundamentals and Applications*; Hanser: Munich, 1995.
- (5) Decker, C. Photoinitiated crosslinking polymerisation. *Prog. Polym. Sci.* **1996**, *21*, 593–650.
- (6) Decker, C. Kinetic study and new applications of UV radiation curing. *Macromol. Rapid Commun.* **2002**, *23*, 1067–1093.
- (7) Stansbury, J. W. Dimethacrylate network formation and polymer property evolution as determined by the selection of monomers and curing conditions. *Dent. Mater.* **2012**, *28*, 13–22.
- (8) Lu, H.; Stansbury, J. W.; Bowman, C. N. Towards the elucidation of shrinkage stress development and relaxation in dental composites. *Dent. Mater.* **2004**, *20*, 979–986.
- (9) De Belder, K.; Pintelon, R.; Demol, C.; Roose, P. Estimation of the equivalent complex modulus of laminated glass beams and its application to sound transmission loss prediction. *Mech. Syst. Signal Process.* **2010**, *24*, 809–822.

- (10) Chartrain, N. A.; Williams, C. B.; Whittington, A. R. A review on fabricating tissue scaffolds using vat photopolymerization. *Acta Biomater.* **2018**, *74*, 90–111.
- (11) Houben, A.; Pien, N.; Lu, X.; Bisi, F.; Van Hoorick, J.; Boone, M. N.; Roose, P.; Van den Bergen, H.; Bontinck, D.; Bowden, T.; et al. Indirect solid freeform fabrication of an initiator-free photocrosslinkable hydrogel precursor for the creation of porous scaffolds. *Macromol. Biosci.* **2016**, *16*, 1883–1894.
- (12) Pagac, M.; Hajnys, J.; Ma, Q.-P.; Jancar, L.; Jansa, J.; Stefek, P.; Mesicek, J. A review of vat photopolymerization technology: Materials, applications, challenges, and future trends of 3D printing. *Polymers* **2021**, *13*, 598.
- (13) Crivello, J.; Narayan, R.; Sternstein, S. Fabrication and mechanical characterization of glass fiber reinforced UV-cured composites from epoxidized vegetable oils. *J. Appl. Polym. Sci.* **1997**, *64*, 2073–2087.
- (14) Glauser, T.; Johansson, M.; Hult, A. Electron-beam curing of thick thermoset composite matrices. *Polymer* **1999**, *40*, 5297–5302.
- (15) Hasiaoui, B.; Ibrahim, A.; L'Hostis, G.; Gautier, K.; Allonas, X.; Croutxé-Barghorn, C.; Durand, B.; Laurent, F. Free radical photopolymerization process for fiber-reinforced polymer: Effect on the mechanical properties. *Polym. Adv. Technol.* **2019**, *30*, 902–909.
- (16) Fu, G.; Kyu, T. Effect of side-chain branching on enhancement of ionic conductivity and capacity retention of a solid copolymer electrolyte membrane. *Langmuir* **2017**, *33*, 13973–13981.
- (17) Fertier, L.; Koleilat, H.; Stemmelen, M.; Giani, O.; Joly-Duhamel, C.; Lapinte, V.; Robin, J.-J. The use of renewable feedstock in UV-curable materials—A new age for polymers and green chemistry. *Prog. Polym. Sci.* **2013**, *38*, 932–962.
- (18) Flory, P. J. *Principles of Polymer Chemistry*; Cornell University Press: Ithaca, New York, 1953.
- (19) Gennes, P.-G. *Scaling Concepts in Polymer Physics* (Cornell University Press: Ithaca, New York, 1979).
- (20) Rubinstein, M.; Colby, R. H. *Polymer Physics*; Oxford University Press: New York, 2003.
- (21) Horkay, F.; McKenna, G. B. *Polymer Networks and Gels. In Physical Properties of Polymers Handbook*; Springer: New York, 2007.
- (22) Danielsen, S. P. O.; Beech, H. K.; Wang, S.; El-Zaatar, B. M.; Wang, X.; Sapir, L.; Ouchi, T.; Wang, Z.; Johnson, P. N.; Hu, Y.; et al. Molecular characterization of polymer networks. *Chem. Rev.* **2021**, *121*, 5042–5092.
- (23) Wang, R.; Alexander-Katz, A.; Johnson, J. A.; Olsen, B. D. Universal cyclic topology in polymer networks. *Phys. Rev. Lett.* **2016**, *116*, No. 188302.
- (24) Wang, R.; Johnson, J. A.; Olsen, B. D. Odd–even effect of junction functionality on the topology and elasticity of polymer networks. *Macromolecules* **2017**, *50*, 2556–2564.
- (25) Anseth, K. S.; Wang, C. M.; Bowman, C. N. Reaction behaviour and kinetic constants for photopolymerizations of multi (meth)acrylate monomers. *Polymer* **1994**, *35*, 3243–3250.
- (26) Di Lorenzo, F.; Seiffert, S. Nanostructural heterogeneity in polymer networks and gels. *Polym. Chem.* **2015**, *6*, 5515–5528.
- (27) Brett, C. J.; Montani, S.; Schwartzkopf, M.; van Benthem, R.; Jansen, J.; Griffini, G.; Roth, S. V.; Johansson, M. K. G. Revealing structural evolution occurring from photo-initiated polymer network formation. *Commun. Chem.* **2020**, *3*, 88.
- (28) Hutchison, J. B.; Anseth, K. S. Off-Lattice Approach to Simulate Radical Chain Polymerizations of Tetrafunctional Monomers. *Macromol. Theory Simul.* **2001**, *10*, 600–607.
- (29) Torres-Knoop, A.; Kryven, I.; Schamboeck, V.; Iedema, P. D. Modeling the free-radical polymerization of hexanediol diacrylate (HDDA): a molecular dynamics and graph theory approach. *Soft Matter* **2018**, *14*, 3404–3414.
- (30) Torres-Knoop, A.; Schamboeck, V.; Govindarajan, N.; Iedema, P. D.; Kryven, I. Effect of different monomer precursors with identical functionality on the properties of the polymer network. *Commun. Mater.* **2021**, *2*, 50.
- (31) Li, C.; Strachan, A. Evolution of network topology of bifunctional epoxy thermosets during cure and its relationship to thermo-mechanical properties: A molecular dynamics study. *Polymer* **2015**, *75*, 151–160.
- (32) Zhong, M.; Wang, R.; Kawamoto, K.; Olsen, B. D.; Johnson, J. A. Quantifying the impact of molecular defects on polymer network elasticity. *Science* **2016**, *353*, 1264–1268.
- (33) Chiou, B.-S.; Khan, S. A. Real-time FTIR and in situ rheological studies on the UV curing kinetics of thiol-ene polymers. *Macromolecules* **1997**, *30*, 7322–7328.
- (34) Lee, S. S.; Luciani, A.; Manson, J.-A. E. A rheological characterisation technique for fast UV-curable systems. *Prog. Org. Coat.* **2000**, *38*, 193–197.
- (35) Steeman, P. A. M.; Dias, A. A.; Wienke, D.; Zwartkuis, T. Polymerization and network formation of UV-curable systems monitored by hyphenated real-time dynamic mechanical analysis and near-infrared spectroscopy. *Macromolecules* **2004**, *37*, 7001–7007.
- (36) Schmidt, C.; Scherzer, T. Monitoring of the shrinkage during the photopolymerization of acrylates using hyphenated photorheometry/near-infrared spectroscopy. *J. Polym. Sci., Part B: Polym. Phys.* **2015**, *53*, 729–739.
- (37) Gorsche, C.; Harikrishna, R.; Baudis, S.; Knaack, P.; Husar, B.; Laeuger, J.; Hoffmann, H.; Liska, R. Real time-NIR/MIR-photorheology: A versatile tool for the in situ characterization of photopolymerization reactions. *Anal. Chem.* **2017**, *89*, 4958–4968.
- (38) Botella, A.; Dupuy, J.; Roche, A. A.; Sautereau, H.; Verney, V. Photo-Rheometry/NIR Spectrometry: An in situ Technique for Monitoring Conversion and Viscoelastic Properties during Photopolymerization. *Macromol. Rapid Commun.* **2004**, *25*, 1155–1158.
- (39) Mayo, S. L.; Olafson, B. D.; Goddard, W. A. DREIDING: a generic force field for molecular simulations. *J. Phys. Chem. A* **1990**, *94*, 8897–8909.
- (40) Gasteiger, J.; Marsili, M. Iterative partial equalization of orbital electronegativity—a rapid access to atomic charges. *Tetrahedron* **1980**, *36*, 3219–3228.
- (41) Samoletov, A. A.; Dettmann, C. P.; Chaplain, M. A. J. Thermostats for “slow” configurational modes. *J. Stat. Phys.* **2007**, *128*, 1321–1336.
- (42) Roose, P.; Vermoesen, E.; Van Vlierberghe, S. Non-steady scaling model for the kinetics of the photo-induced free radical polymerization of crosslinking networks. *Polym. Chem.* **2020**, *11*, 2475–2484.
- (43) Roose, P.; Van den Bergen, H.; Houben, A.; Bontinck, D.; Van Vlierberghe, S. A semiempirical scaling model for the solid-and liquid-state photopolymerization kinetics of semicrystalline acrylated oligomers. *Macromolecules* **2018**, *51*, 5027–5038.
- (44) Doherty, D. C.; Holmes, B. N.; Leung, P.; Ross, R. B. Polymerization molecular dynamics simulations. I. Cross-linked atomistic models for poly(methacrylate) networks. *Comput. Theor. Polym. Sci.* **1998**, *8*, 169–178.
- (45) Leung, Y.-K.; Eichinger, B. E. Computer simulation of end-linked elastomers. II. Bulk cured tetrafunctional networks. *J. Chem. Phys.* **1984**, *80*, 3885–3891.
- (46) Yang, S.; Qu, J. Computing thermomechanical properties of crosslinked epoxy by molecular dynamic simulations. *Polymer* **2012**, *53*, 4806–4817.
- (47) Hassan, W. A. W.; Liu, J.; Howlin, B. J.; Ishida, H.; Hamerton, I. Examining the influence of bisphenol A on the polymerisation and network properties of an aromatic benzoxazine. *Polymer* **2016**, *88*, 52–62.
- (48) Gou, J.; Minaie, B.; Wang, B.; Liang, Z.; Zhang, C. Computational and experimental study of interfacial bonding of single-walled nanotube reinforced composites. *Comput. Mater. Sci.* **2004**, *31*, 225–236.
- (49) Heine, D. R.; Grest, G. S.; Lorenz, C. D.; Tsige, M.; Stevens, M. J. Atomistic simulations of end-linked poly(dimethylsiloxane) networks: structure and relaxation. *Macromolecules* **2004**, *37*, 3857–3864.
- (50) Li, C.; Strachan, A. Molecular simulations of crosslinking process of thermosetting polymers. *Polymer* **2010**, *51*, 6058–6070.
- (51) Wu, C.; Xu, W. Atomistic molecular modelling of crosslinked epoxy resin. *Polymer* **2006**, *47*, 6004–6009.

- (52) Wu, C.; Xu, W. Atomistic molecular simulations of structure and dynamics of crosslinked epoxy resin. *Polymer* **2007**, *48*, 5802–5812.
- (53) Farah, K.; Karimi-Varzaneh, H. A.; Müller-Plathe, F.; Böhm, M. C. Reactive molecular dynamics with material-specific coarse-grained potentials: Growth of polystyrene chains from styrene monomers. *J. Phys. Chem. B* **2010**, *114*, 13656–13666.
- (54) Saiev, S.; Bonnaud, L.; Dumas, L.; Zhang, T.; Dubois, P.; Beljonne, D.; Lazzaroni, R. Do carbon nanotubes improve the thermomechanical properties of benzoxazine thermosets? *ACS Appl. Mater. Interfaces* **2018**, *10*, 26669–26677.
- (55) Saiev, S.; Bonnaud, L.; Dubois, P.; Beljonne, D.; Lazzaroni, R. Modeling the formation and thermomechanical properties of polybenzoxazine thermosets. *Polym. Chem.* **2017**, *8*, 5988–5999.
- (56) Saiev, S.; Bonnaud, L.; Zúñiga, C.; Dubois, P.; Beljonne, D.; Ronda, J. C.; Cadiz, V.; Lazzaroni, R. Positive effect of functional side groups on the structure and properties of benzoxazine networks and nanocomposites. *Polym. Chem.* **2019**, *10*, 5251–5264.
- (57) Scanlan, J. The effect of network flaws on the elastic properties of vulcanizates. *J. Polym. Sci.* **1960**, *43*, 501–508.
- (58) Case, L. C. Branching in polymers. I. Network defects. *J. Polym. Sci.* **1960**, *45*, 397–404.
- (59) Korolev, G. V.; Mogilevich, M. M. *Three-Dimensional Free-Radical Polymerization*; Springer: Berlin, 2009, Chapter 5.
- (60) Mark, J. E.; Tang, M. Y. Dependence of the elastomeric properties of bimodal networks on the lengths and amounts of the short chains. *J. Polym. Sci.: Polym. Phys. Ed.* **1984**, *22*, 1849–1855.
- (61) Tang, M. Y.; Mark, J. E. Effect of composition and cross-link functionality on the elastomeric properties of bimodal networks. *Macromolecules* **1984**, *17*, 2616–2619.
- (62) Kizilay, M. Y.; Okay, O. Effect of hydrolysis on spatial inhomogeneity in poly(acrylamide) gels of various crosslink densities. *Polymer* **2003**, *44*, 5239–5250.
- (63) Lindemann, B.; Schröder, U. P.; Oppermann, W. Influence of the cross-linker reactivity on the formation of inhomogeneities in hydrogels. *Macromolecules* **1997**, *30*, 4073–4077.
- (64) Felderhof, B. U.; Iske, P. Mean-field approximation to the effective elastic moduli of a solid suspension of spheres. *Phys. Rev. A* **1992**, *45*, 611.
- (65) Huber, G.; Vilgis, T. A. On the mechanism of hydrodynamic reinforcement in elastic composites. *Macromolecules* **2002**, *35*, 9204–9210.
- (66) Heinrich, G.; Klüppel, M.; Vilgis, T. A. Reinforcement of elastomers. *Curr. Opin. Solid State Mater. Sci.* **2002**, *6*, 195–203.
- (67) Akagi, Y.; Gong, J. P.; Chung, U.-i.; Sakai, T. Transition between phantom and affine network model observed in polymer gels with controlled network structure. *Macromolecules* **2013**, *46*, 1035–1040.
- (68) Panyukov, S. V. Theory of heterogeneities in polymer networks. *Polym. Sci., Ser. A* **2016**, *58*, 886–898.
- (69) Panyukov, S. V. Theory of flexible polymer networks: Elasticity and heterogeneities. *Polymers* **2020**, *12*, 767.